Journal of Materials Chemistry A

PAPER

View Article Online
View Journal | View Issue

Cite this: J. Mater. Chem. A, 2014, 2, 12507

# Nanoporous covalent organic polymers incorporating Tröger's base functionalities for enhanced $CO_2$ capture†

Jeehye Byun,[a] Sang-Hyun Je,[a] Hasmukh A. Patel,[a] Ali Coskun*[ab] and Cafer T. Yavuz*[a]

Received 10th February 2014
Accepted 29th April 2014

DOI: 10.1039/c4ta00698d

www.rsc.org/MaterialsA

The $CO_2$ uptake capacity and $CO_2/N_2$ selectivity of Tröger's base-bridged nanoporous covalent organic polymers (TB-COPs) were investigated. The TB-COPs were synthesized by reacting the terminal amines of tetrahedral monomers – namely, tetraanilyladamantane and tetraanilylmethane – with dimethoxymethane in a one-pot reaction under relatively mild conditions. Interestingly, these two tetrahedral monomers formed nanoporous polymers with substantially different surface areas. While the polymer resulting from the Trögerization of the tetraanilyladamantane monomer (TB-COP-1) exhibited a high surface area of 1340 $m^2\ g^{-1}$, that from the tetraanilylmethane monomer (TB-COP-2) was found to be only 0.094 $m^2\ g^{-1}$. This unusual phenomenon can be explained by the proximity of the amino moieties to each other within the monomeric unit. A shorter distance between the amino groups enables intramolecular as well as intermolecular cyclization, thus resulting in a much lower porosity. TB-COP-1 exhibited significant $CO_2$ uptake capacities of up to 5.19 and 3.16 mmol $g^{-1}$ at 273 and 298 K under ambient pressure, and $CO_2/N_2$ selectivities of 79.2 and 68.9 at 273 and 298 K at 1 bar for a gas mixture of $CO_2 : N_2$ at a ratio of 0.15 : 0.85. It is noteworthy that TB-COP-1 showed remarkable selectivity retention when increasing the temperature from 273 to 298 K.

## Introduction

Carbon dioxide capture and sequestration (CCS) has undoubtedly been at the forefront of research over the last decade in order to mitigate greenhouse gas problems,[1] leading to many efforts to tackle the growing crisis by developing efficient materials and technologies.[2–8] The commercial CCS methods using aqueous amine solutions have a number of drawbacks such as the inevitable corrosion and energy intensive solvent regeneration.[9] An alternative approach based on pressure or vacuum swing adsorption involving microporous materials is a promising technique for capturing $CO_2$ from flue gas mixtures because of its efficiency and low energy requirements.[10]

Currently, most efforts are focused on establishing efficient and low cost porous materials, including activated carbon,[11] metal–organic frameworks,[4,12,13] silicates,[14] and nanoporous polymeric networks.[3,7] These materials are expected to meet the basic requirements of CCS: (1) water and thermal stability, (2) selectivity over other flue gases, and (3) economic viability. Nanoporous polymeric frameworks, either crystalline or amorphous, have been studied extensively for gas storage and separation, *e.g.*, Schiff base networks (SNWs),[15] benzimidazole-linked polymers (BILPs),[16–18] covalent triazine frameworks (CTFs),[19] polymers with intrinsic microporosity (PIMs),[20–22] porous aromatic frameworks (PAFs),[23] porous polymer networks (PPNs),[24] covalent organic frameworks (COFs),[25,26] porous organic frameworks (POFs),[27] covalent organic polymers (COPs),[28–30] hypercrosslinked and conjugated microporous polymers (HCPs and CMPs),[31,32] elemental organic frameworks (EOFs),[33] microporous organic polymers (MOPs),[34] porous polymer frameworks (PPFs),[35] and others.[36–43]

Tröger's base (TB) is a bridged bicyclic amine,[44,45] and is an excellent candidate for $CO_2$ capture due to the inherent basic character of the tertiary nitrogen functionalities. Recently, Carta *et al.*[46] demonstrated the construction of membranes containing TB linkages in polymers of intrinsic microporosity (PIMs) for high gas permeabilities and selectivities for small gas molecules ($H_2$, $O_2$) over larger ones ($CH_4$, $N_2$). Three-dimensional nanoporous polymers based on TB were also reported by Zhu *et al.*,[47] in which triaminotriptycene was used as a building block for the generation of TB-linked microporous organic polymers (MOPs). These MOPs exhibit $CO_2$ storage capacities of up to 4.05 mmol $g^{-1}$ at 273 K and 1 bar, proving the contribution of basic sites in $CO_2$ binding. The capacity, however, is lower than that of imine-based porous polymer frameworks (PPFs), where 6.07 mmol $g^{-1}$ of $CO_2$ uptake was observed.[35] Although these capacities are significant, both the TB-MOP and

[a]Graduate School of EEWS, Korea Advanced Institute of Science and Technology (KAIST), Daejeon 305-701, Republic of Korea. E-mail: yavuz@kaist.ac.kr
[b]Department of Chemistry, Korea Advanced Institute of Science and Technology (KAIST), Daejeon 305-701, Republic of Korea. E-mail: coskun@kaist.ac.kr

† Electronic supplementary information (ESI) available: Supplementary methods, discussion, Fig. S1–S11, and Table S1–S3. See DOI: 10.1039/c4ta00698d

PPF suffer from low $CO_2/N_2$ selectivities, mostly due to the interplay between porosity and binding energy.

Nanoporous polymers for pressure or vacuum swing adsorption are expected to be robust and insoluble in order to survive the regeneration conditions. One way to achieve the desired material qualities is to employ tetrahedral monomers in the preparation of nanoporous polymers in order to establish permanent and highly porous structures. Here, we report two new TB-linked covalent organic polymers (TB-COPs) incorporating tetrahedral building blocks, namely tetraanilyladamantane (TB-COP-1) and tetraanilylmethane (TB-COP-2). While TB-COP-1 undergoes intermolecular cyclization, TB-COP-2 prefers intramolecular along with intermolecular cyclization due to the proximity of the amino moieties in the tetraanilylmethane monomer, pointing to the fact that both the rigidity of the monomer and the distance between the amino groups are very important in the synthesis of Tröger's base-linked covalent organic polymers. Unlike previous porous polymers incorporating Tröger's base, TB-COP-1 exhibits superior $CO_2$ uptake of up to 5.19 mmol $g^{-1}$ at 273 K without compromising its $CO_2/N_2$ selectivity (79.2 at 273 K, 1 bar), which is one of the highest reported $CO_2$ adsorptions. The selectivity is good compared with other organic porous materials, and is closely comparable to those of metal organic frameworks (MOFs). With the exception of the recently reported azo-linked covalent organic polymers (azo-COPs),[48] the $CO_2/N_2$ selectivity in porous solids decreases with rising temperature, in some cases by up to 50%. TB-COPs, however, exhibit significant $CO_2/N_2$ selectivity retention (only a ~10% decrease) with an increase in temperature from 273 to 298 K. Interestingly, we also observed that the internally cyclized and non-porous (based on $N_2$ BET) TB-COP-2 also showed moderate $CO_2$ uptake.

## Results and discussion

Tetrahedral building blocks offer easy and immediate access to a superstructure, regardless of the kinetics of polymeric assembly, thus leading to maximal void formation.[23,24] In this work, we compared (Scheme 1) tetraphenylmethane and tetraphenyladamantane cores in the formation TB-COPs. The tetraphenyladamantane core offers a more rigid tetrahedral system as the phenylene legs are not as free to swing as in a tetraphenylmethane block. In addition, the reactive amine sites are well separated, thus minimizing potential intramolecular cyclization. The TB-COPs are prepared *via* a one-pot polymerization of tetraanilylmethane or tetraanilyladamantane with dimethoxymethane in the presence of trifluoroacetic acid, both as a catalyst and as a solvent, under a nitrogen atmosphere at room temperature.[46] The *in situ* formation of formaldehyde moieties enables the alkylation and subsequent cyclization of the amino groups to form corresponding amorphous crosslinked polymers bridged by Tröger's base. Rapid precipitation of the TB-COPs was observed after 1 h in trifluoroacetic acid. The TB-COPs were found to be insoluble in any of the common organic solvents.

In order to verify the formation of the TB-COPs, we carried out cross-polarization magic-angle spinning (CP/MAS) $^{13}C$ NMR, Fourier transform infrared spectroscopy (FTIR) and elemental analysis. The CP/MAS $^{13}C$ NMR spectrum of TB-COP-1 showed peaks located at 145.5, 123.7, 67.4, 59.1, 46.85, and 38.7 ppm, clearly indicating the formation of Tröger's base linkages (Fig. 1A).[46] The chemical shifts located at 38.7 and 46.85 ppm are attributed to the secondary and tertiary carbon atoms in the symmetric adamantane core, and the chemicals shifts at 67.4 and 59.1 ppm are attributed to the carbon atoms within the Tröger's base. The chemical shifts from the phenyl groups in TB-COP-1 are observed as two broad peaks at 145.5 and 123.7 ppm due to the highly symmetric structure of the polymer. In TB-COP-2, however, chemical shifts are observed at 166.8, 152.35, 135, 123.3, 70, 63, and 56.3 ppm (Fig. 1B). The chemical shifts located at 63.0 and 56.3 indicate the formation of Tröger's base linkages. The broad distribution of the aromatic peaks points to the lack of symmetry in the aromatic carbons, which is an indication of random intramolecular cyclization, thus resulting in the formation of a non-porous polymer structure.

The characteristic C–N stretching bands located at 1330 and 1043 $cm^{-1}$ in the FTIR spectra of the TB-COPs prove the formation of Tröger's base linkages (see ESI, Fig. S1†). Moreover, the intensity of the stretching bands associated with the aromatic amines, located at around 3400 to 3200 $cm^{-1}$, are reduced significantly after the formation of the TB-COPs. The –OH stretching band located at 3686 $cm^{-1}$ in the FTIR spectra of the TB-COPs is attributed to the water molecules trapped during post-synthetic work-up. The formation of the TB-COPs was also verified (see ESI, Table S1†) using elemental analysis. The elemental analysis of the TB-COPs is in good accord with the theoretical composition. The oxygen content in the experimental analysis was mainly attributed to trapped moisture/air

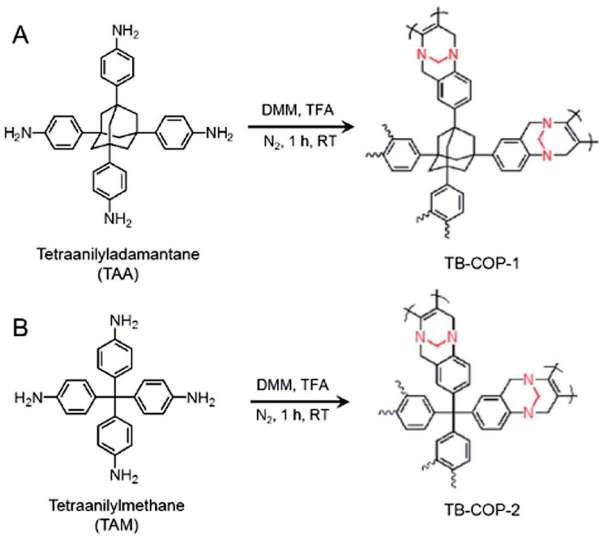


Scheme 1 Proposed chemical structures of (A) TB-COP-1 and (B) TB-COP-2 along with the tetrahedral monomers tetraanilyladamantane (TAA) and tetraanilylmethane (TAM). TB-COPs were synthesized by reacting aromatic amines with dimethoxymethane (DMM) in the presence of trifluoroacetic acid (TFA) for 1 h under a nitrogen atmosphere at room temperature.

 

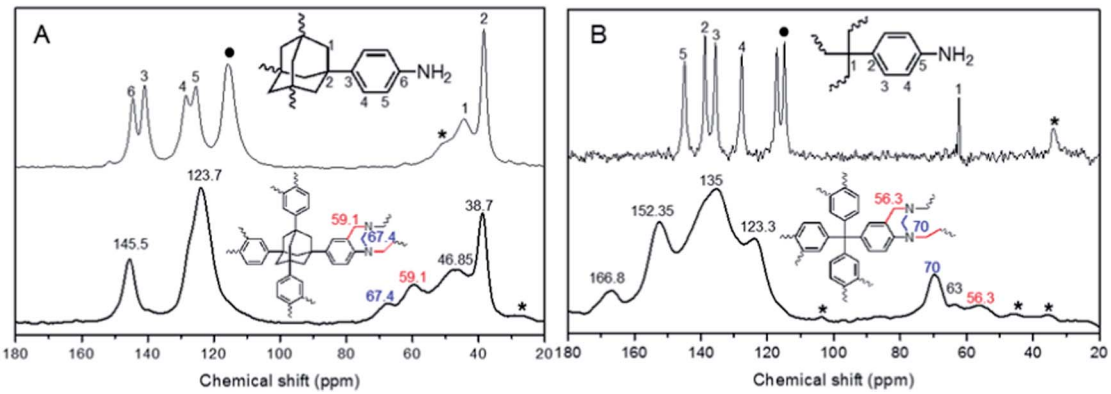


Fig. 1 Solid-state CP/MAS $^{13}$C-NMR spectrum of (A) TB-COP-1, (B) TB-COP-2 and their starting materials with the assignments of the respective bonds. Black asterisks (*) indicate spinning side bands, and solid circles (●) indicate the terminal C–$NH_2$ bonds at 115 ppm.

in the TB-COPs, and is commonly observed in porous materials.[49]

The pore structure of the TB-COPs was measured (Fig. 2A) by $N_2$ physisorption measurements at 77 K. TB-COP-1 is microporous and exhibits a conventional type I reversible adsorption isotherm. We were not able to measure the $N_2$ adsorption data for TB-COP-2 at high relative pressure because of its negligible adsorption. The Brunauer–Emmett–Teller (BET) surface areas were 1340 $m^2\ g^{-1}$ for TB-COP-1, and 0.094 $m^2\ g^{-1}$ for TB-COP-2 (see ESI, Fig. S3†). The total pore volume of TB-COP-1 was 0.541 $cm^3\ g^{-1}$, and the micropore surface area, estimated by *t*-plot method, was 772.4 $m^2\ g^{-1}$. The microporosity ($V_{micro}/V_{total}$, where $V_{micro}$ is micropore volume and $V_{total}$ is total pore volume) of TB-COP-1 was found to be 0.58, indicating that the majority of the pores are in the microporous region. The NLDFT (Non-Local Density Functional Theory) pore size distribution of TB-COP-1 is narrow with an average pore size of 1.58 nm. These pore characteristics put TB-COP-1 in the same league as well-known microporous materials with high surface areas such as zeolites and MOFs.[13,50,51]

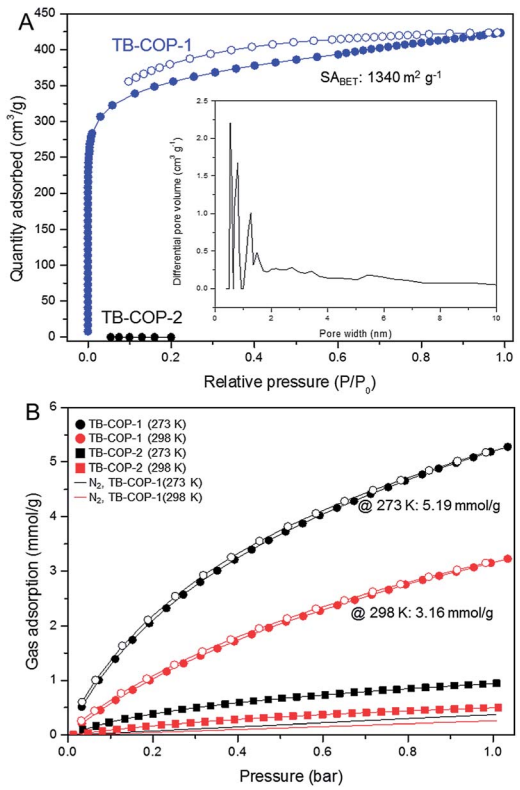


Fig. 2 (A) $N_2$ adsorption–desorption isotherm measured at 77 K (inset: pore size *versus* differential pore volume of TB-COP-1). (B) Low pressure $CO_2$ and $N_2$ adsorptions for TB-COP-1 and TB-COP-2 at 273 K (black) and 298 K (red) up to 1 bar. Closed markers (●) indicate gas adsorption and open markers (○) indicate gas desorption.

Tröger's base is known to form (Scheme 2A) through a concerted iminization of an amine that is followed by a nucleophilic attack on the imine intermediate.[52] Two key steps are responsible for the bent, butterfly-like ring system that forms. The first is the electrophilic aromatic substitution of the charged iminium intermediate. The second is the attack of a neighbouring amine group on a second iminium ion that forms following the first step. In TB-COP-1, the mechanism should follow (Scheme 2B) a traditional Tröger's base formation path (Route I), as is evident from the NMR spectrum and its high surface area. In the case of TB-COP-2, however, it is very hard to predict the TB formation mechanism. As observed in the $^{13}$C NMR, a wide range of carbon atoms with different environments is present. These findings lead us to believe that one or both of the steps in the Tröger's base formation must have an alternative pathway, resulting in a non-porous solid with the correct functional groups. We have proposed (Scheme 2C) a plausible mechanism for the formation of TB-COP-2 in order to understand its non-porous nature. We believe that the second iminium ion, which is formed following the first step, can react with an amino group *via* Route I and/or Route II. The relatively rigid adamantane core is expected to prevent this alternative (Route II) intramolecular Tröger's base formation by restricting the swing of the phenylene units, which leads to only intermolecular polymerization, resulting in a high surface area. On the contrary, the carbon core of the tetraanilylmethane, due to its relatively flexible nature, showed a complex mixture of mechanisms leading to a negligible surface area, suggesting

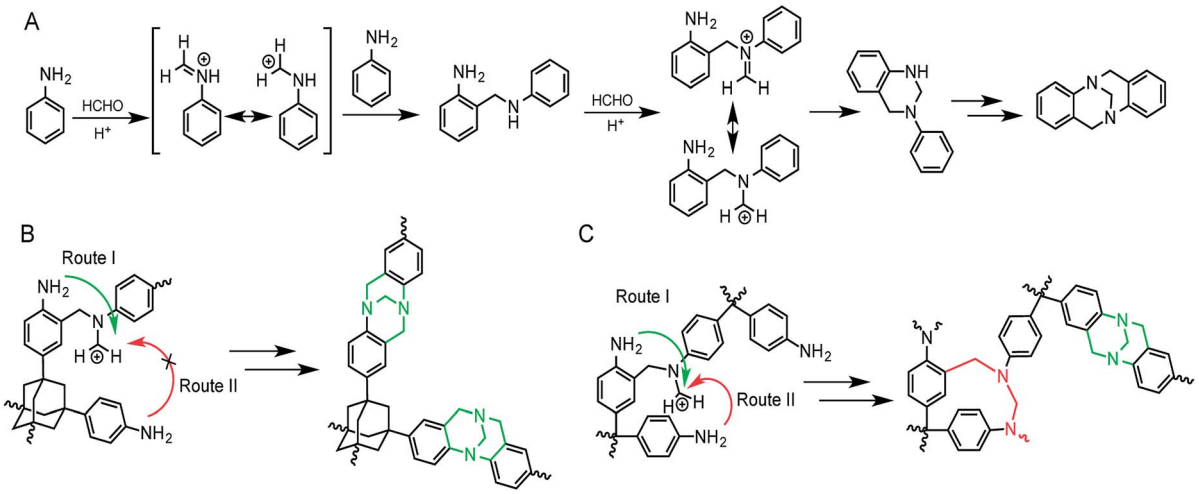


Scheme 2 (A) Traditional Tröger's base formation mechanism. Proposed formation mechanisms of TB-COP-1 (B) and TB-COP-2 (C). While TB-COP-1 can only undergo intermolecular (Route I) Tröger's base formation due to its rigid structure, TB-COP-2 can react in both an inter-(Route I) and intra-(Route II) molecular fashion.

that both inter-(Route I) and intra-(Route II) molecular Tröger's base formations are possible thus forming an almost non-porous framework. In an attempt to quantify Route I over Route II, we calculated the expected and experimental C/N ratios (Table S1†). Route II would increase the carbon content and thus the C/N ratio because of the additional methylene–$CH_2$ bridges formed *via* intramolecular cyclizations (Scheme S1†). TB-COP-2 has a higher experimental C/N ratio than expected, revealing a higher Route II contribution compared to Route I. TB-COP-1 has a lower experimental C/N ratio than the theoretical value, an expected result considering oxygen contamination.

The thermal stability of the TB-COPs, one of the vital parameters for their potential application in commercial CCS technology, was measured (Fig. S4†) by thermogravimetric analysis (TGA). TB-COP-1 turned out to be stable up to 430 °C and 350 °C in inert and oxidative environments, respectively. The initial loss of mass before 250 °C is attributed to the release of trapped solvents. TB-COP-2 started to decompose at 380 °C under both inert and oxidative conditions. The powder X-ray diffraction patterns of the TB-COPs show (Fig. S5†) amorphous polymeric structures. The morphology of the TB-COPs was measured by field emission scanning electron microscopy, which reveals (Fig. S6†) the formation of irregular micron-sized particles after polymerization. Micron-sized particles are often preferred industrially for fluidized bed adsorption applications.

The inherent microporosity and nitrogen-rich structure of the TB-COPs was utilized for $CO_2$ capture. The $CO_2$ uptakes of the TB-COPs were measured (Fig. 2B) at 273 and 298 K up to 1 bar. All the adsorption measurements were carried out after degassing the TB-COPs at 150 °C for 5 hours, and the measurements were repeated at least three times with different batches of samples to ensure reproducibility of the gas adsorption data. The $CO_2$ isotherms show an adsorption capacity of 5.19 mmol $g^{-1}$ (22.84 wt%) for TB-COP-1, and 0.95 mmol $g^{-1}$ (4.18 wt%) for TB-COP-2 at 273 K. At 298 K, the $CO_2$ uptake of the TB-COPs decreased to 3.16 mmol $g^{-1}$ (13.91 wt%) for TB-COP-1, and 0.5 mmol $g^{-1}$ (2.2 wt%) for TB-COP-2. The $CO_2$ adsorption capacity of TB-COP-1 at 273 K is comparable to the nanoporous polymeric networks with the highest reported $CO_2$ uptakes, such as PPF-1 (6.07 mmol $g^{-1}$),[35] BILP-4 (5.34 mmol $g^{-1}$)[53] and TB-MOP (4.05 mmol $g^{-1}$)[47] (see ESI, Table S3† for a more comprehensive data set). Despite its non-porous structure, TB-COP-2 also exhibits moderate $CO_2$ uptake, thanks to its $CO_2$-philic framework. The good adsorption of $CO_2$ onto the TB-COP-2 structure led us to examine the surface area derived from the $CO_2$ isotherms (Fig. S7†). This approach is commonly exercised when the $N_2$ probe cannot access the depths of $CO_2$-philic solids.[54] For TB-COP-2, which has almost no $N_2$ surface area, the BET surface area from the $CO_2$ adsorption was found to be 154.4 $m^2$ $g^{-1}$ and 100.6 $m^2$ $g^{-1}$ at 273 K and 298 K, respectively. For TB-COP-1, the $CO_2$ surface area was 694.9 $m^2$ $g^{-1}$ and 599.7 $m^2$ $g^{-1}$ at 273 K and 298 K, respectively.

A relatively small hysteresis in the $CO_2$ adsorption–desorption isotherms for the TB-COPs, indicates that the interactions between the adsorbent and the $CO_2$ gas molecules are weak. This weak interaction is crucial for the regeneration of the adsorbents without the need for energy-intensive operations. The isosteric heat of adsorption ($Q_{st}$) of the TB-COPs was calculated (Fig. 3A and S8†) from the $CO_2$ uptake data at 273 and 298 K by using the Clausius–Clapeyron equation. The $Q_{st}$ values of TB-COP-1 and TB-COP-2 are 25.95 kJ $mol^{-1}$ and 33.07 kJ $mol^{-1}$, respectively, which are well below the values expected for a chemisorption process (>40 kJ $mol^{-1}$). Therefore, the high $CO_2$ affinity of the TB-COPs is mainly attributed to the inherent microporosity of TB-COP-1 and the enhanced dipole–quadrupole interaction between the quadrupole moment of the $CO_2$ molecules and the nitrogen-rich polar binding sites on the TB-COP structures.[48]

The selectivity of $CO_2$ over $N_2$ gas is a necessity for CCS processes as the flue gases contain up to 85% $N_2$ gas. So far, to

 

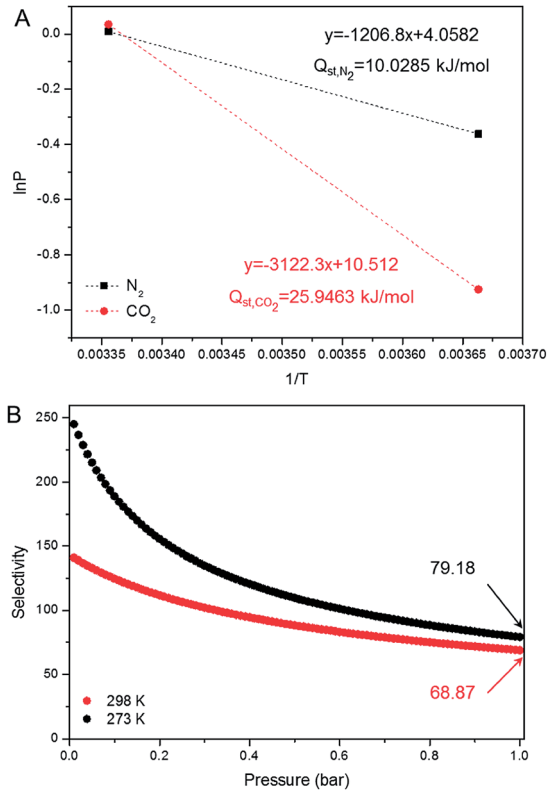


Fig. 3 (A) Gas adsorption data of TB-COP-1 fitted with the Clausius–Clapeyron equation ($\Delta H = R[\partial \ln P/\partial(1/T)]_\theta$) for calculation of the isosteric heat of adsorption ($Q_{st}$). (B) $CO_2/N_2$ selectivity of TB-COP-1 predicted *via* Ideal Adsorption Solution Theory (IAST).

the best of our knowledge, porous organic polymers with extremely high $CO_2$ uptake display mediocre selectivity over $N_2$ gas, and the selectivity becomes even lower on increasing the temperature from 273 K to 298 K.[35,53] Therefore, $N_2$ uptake studies of the TB-COPs were also performed to determine their selective adsorption behavior. The selectivities were calculated by Ideal Adsorbed Solution Theory (IAST) (Fig. 3B) and the IAST selectivities were predicted for a 0.15 : 0.85 $CO_2$ and $N_2$ mixture. The $CO_2/N_2$ selectivities were only calculated for TB-COP-1 because of the inability to record $N_2$ adsorption data for TB-COP-2 despite using large amounts of adsorbent. The IAST $CO_2/N_2$ selectivity of TB-COP-1 was 79.2 and 68.9 at 273 and 298 K, respectively, at 1 bar. Interestingly, TB-COP-1 showed remarkable selectivity retention with increasing temperature compared with other porous polymers (Table S3†).

## Conclusions

Nanoporous covalent organic polymers bearing 3D architectures, high surface areas and Tröger's base functionalities were synthesized in a simple one-pot reaction. We note that the relatively rigid adamantane core prevented intramolecular Tröger's base formations by restricting the swing of the phenylene legs whilst the carbon core of tetraphenylmethane resulted in a complex mixture of mechanisms leading to a negligible surface area, indicating that intra- and inter-molecular Tröger's base formations randomly occur. These findings point to the fact that porous polymers incorporating TB functionalities should possess monomers with rigid backbones and well-separated amino groups for high-surface area and high uptake capacity. Future directions may include the cross combination of the cores and utilization of linkers with other 1D or 2D geometries. These attempts would enhance, for example, the nitrogen content of the resulting product, enabling higher $CO_2$ uptake. Challenges exist, however, since the internal Tröger's base formation mechanism we described here may alter the formation of the desired permanent pores.

## Acknowledgements

C.T.Y. acknowledges the financial support by grants from Korea CCS R&D Centre, Basic Science Research Program through the National Research Foundation of Korea (NRF) funded by the Ministry of Science, ICT & Future Planning (2013R1A1A1012998), IWT (NRF-2012-C1AAA001-M1A2A2026588), and WCU programme (R31-2008-000-10055-0) funded by the Ministry of Education, Science and Technology of Korean government, and KAIST EEWS Initiative. A.C. acknowledges the support from the KUSTAR-KAIST Institute, Korea, under the R&D programme supervised by the KAIST and Basic Science Research Program through the National Research Foundation of Korea (NRF) funded by the Ministry of Science, ICT & Future Planning (2013R1A1A1012282). J.B. thanks the National Research Foundation of Korea (NRF) for a global Ph.D. fellowship (2013H1A2A1033423).

## Notes and references

1 D. M. D'Alessandro, B. Smit and J. R. Long, *Angew. Chem., Int. Ed.*, 2010, **49**, 6058–6082.
2 S. Choi, J. H. Drese, P. M. Eisenberger and C. W. Jones, *Environ. Sci. Technol.*, 2011, **45**, 2420–2427.
3 R. Dawson, A. I. Cooper and D. J. Adams, *Prog. Polym. Sci.*, 2012, **37**, 530–563.
4 G. Ferey, *Chem. Soc. Rev.*, 2008, **37**, 191–214.
5 H. K. He, W. W. Li, M. J. Zhong, D. Konkolewicz, D. C. Wu, K. Yaccato, T. Rappold, G. Sugar, N. E. David and K. Matyjaszewski, *Energy Environ. Sci.*, 2013, **6**, 488–493.
6 H. K. He, M. J. Zhong, D. Konkolewicz, K. Yacatto, T. Rappold, G. Sugar, N. E. David, J. Gelb, N. Kotwal, A. Merkle and K. Matyjaszewski, *Adv. Funct. Mater.*, 2013, **23**, 4720–4728.
7 A. Thomas, *Angew. Chem., Int. Ed.*, 2010, **49**, 8328–8344.
8 Z. H. Xiang, X. Zhou, C. H. Zhou, S. Zhong, X. He, C. P. Qin and D. P. Cao, *J. Mater. Chem.*, 2012, **22**, 22663–22669.
9 S. Zulfiqar, F. Karadas, J. Park, E. Deniz, G. D. Stucky, Y. Jung, M. Atilhan and C. T. Yavuz, *Energy Environ. Sci.*, 2011, **4**, 4528–4531.
10 E. Deniz, F. Karadas, H. A. Patel, S. Aparicio, C. T. Yavuz and M. Atilhan, *Microporous Mesoporous Mater.*, 2013, **175**, 34–42.
11 M. Sevilla, C. Falco, M. M. Titirici and A. B. Fuertes, *RSC Adv.*, 2012, **2**, 12792–12797.

12 S. Kitagawa, R. Kitaura and S. Noro, *Angew. Chem., Int. Ed.*, 2004, **43**, 2334–2375.
13 O. M. Yaghi, M. O'Keeffe, N. W. Ockwig, H. K. Chae, M. Eddaoudi and J. Kim, *Nature*, 2003, **423**, 705–714.
14 T. H. Bae, M. R. Hudson, J. A. Mason, W. L. Queen, J. J. Dutton, K. Sumida, K. J. Micklash, S. S. Kaye, C. M. Brown and J. R. Long, *Energy Environ. Sci.*, 2013, **6**, 128–138.
15 M. G. Schwab, B. Fassbender, H. W. Spiess, A. Thomas, X. L. Feng and K. Mullen, *J. Am. Chem. Soc.*, 2009, **131**, 7216–7217.
16 M. G. Rabbani and H. M. El-Kaderi, *Chem. Mater.*, 2011, **23**, 1650–1653.
17 M. G. Rabbani, T. E. Reich, R. M. Kassab, K. T. Jackson and H. M. El-Kaderi, *Chem. Commun.*, 2012, **48**, 1141–1143.
18 M. G. Rabbani, A. K. Sekizkardes, O. M. El-Kadri, B. R. Kaafarani and H. M. El-Kaderi, *J. Mater. Chem.*, 2012, **22**, 25409–25417.
19 P. Kuhn, M. Antonietti and A. Thomas, *Angew. Chem., Int. Ed.*, 2008, **47**, 3450–3453.
20 N. B. McKeown and P. M. Budd, *Chem. Soc. Rev.*, 2006, **35**, 675–683.
21 N. B. McKeown and P. M. Budd, *Macromolecules*, 2010, **43**, 5163–5176.
22 N. B. McKeown, S. Hanif, K. Msayib, C. E. Tattershall and P. M. Budd, *Chem. Commun.*, 2002, **23**, 2782–2783.
23 T. Ben, H. Ren, S. Q. Ma, D. P. Cao, J. H. Lan, X. F. Jing, W. C. Wang, J. Xu, F. Deng, J. M. Simmons, S. L. Qiu and G. S. Zhu, *Angew. Chem., Int. Ed.*, 2009, **48**, 9457–9460.
24 D. Q. Yuan, W. G. Lu, D. Zhao and H. C. Zhou, *Adv. Mater.*, 2011, **23**, 3723–3725.
25 J. W. Colson and W. R. Dichtel, *Nat. Chem.*, 2013, **5**, 453–465.
26 H. M. El-Kaderi, J. R. Hunt, J. L. Mendoza-Cortes, A. P. Cote, R. E. Taylor, M. O'Keeffe and O. M. Yaghi, *Science*, 2007, **316**, 268–272.
27 A. P. Katsoulidis and M. G. Kanatzidis, *Chem. Mater.*, 2011, **23**, 1818–1824.
28 H. A. Patel, S. H. Je, J. Park, D. P. Chen, Y. Jung, C. T. Yavuz and A. Coskun, *Nat. Commun.*, 2013, **4**, 1357.
29 H. A. Patel, F. Karadas, J. Byun, J. Park, E. Deniz, A. Canlier, Y. Jung, M. Atilhan and C. T. Yavuz, *Adv. Funct. Mater.*, 2013, **23**, 2270–2276.
30 H. A. Patel, F. Karadas, A. Canlier, J. Park, E. Deniz, Y. Jung, M. Atilhan and C. T. Yavuz, *J. Mater. Chem.*, 2012, **22**, 8431–8437.
31 R. Dawson, D. J. Adams and A. I. Cooper, *Chem. Sci.*, 2011, **2**, 1173–1177.
32 R. Dawson, T. Ratvijitvech, M. Corker, A. Laybourn, Y. Z. Khimyak, A. I. Cooper and D. J. Adams, *Polym. Chem.*, 2012, **3**, 2034–2038.
33 M. Rose, W. Bohlmann, M. Sabo and S. Kaskel, *Chem. Commun.*, 2008, **21**, 2462–2464.
34 O. K. Farha, A. M. Spokoyny, B. G. Hauser, Y. S. Bae, S. E. Brown, R. Q. Snurr, C. A. Mirkin and J. T. Hupp, *Chem. Mater.*, 2009, **21**, 3033–3035.
35 Y. L. Zhu, H. Long and W. Zhang, *Chem. Mater.*, 2013, **25**, 1630–1635.
36 S. Y. Ding and W. Wang, *Chem. Soc. Rev.*, 2013, **42**, 548–568.
37 N. Y. Du, H. B. Park, M. M. Dal-Cin and M. D. Guiver, *Energy Environ. Sci.*, 2012, **5**, 7306–7322.
38 N. Y. Du, H. B. Park, G. P. Robertson, M. M. Dal-Cin, T. Visser, L. Scoles and M. D. Guiver, *Nat. Mater.*, 2011, **10**, 372–375.
39 E. A. Jackson, Y. Lee and M. A. Hillmyer, *Macromolecules*, 2013, **46**, 1484–1491.
40 J. L. Novotney and W. R. Dichtel, *ACS Macro Lett.*, 2013, **2**, 423–426.
41 P. Pandey, O. K. Farha, A. M. Spokoyny, C. A. Mirkin, M. G. Kanatzidis, J. T. Hupp and S. T. Nguyen, *J. Mater. Chem.*, 2011, **21**, 1700–1703.
42 D. C. Wu, F. Xu, B. Sun, R. W. Fu, H. K. He and K. Matyjaszewski, *Chem. Rev.*, 2012, **112**, 3959–4015.
43 Z. J. Yan, H. Ren, H. P. Ma, R. R. Yuan, Y. Yuan, X. Q. Zou, F. X. Sun and G. S. Zhu, *Microporous Mesoporous Mater.*, 2013, **173**, 92–98.
44 J. Tröger, *Journal für Praktische Chemie*, 1887, **36**, 225–245.
45 M. A. Spielman, *J. Am. Chem. Soc.*, 1935, **57**, 583–585.
46 M. Carta, R. Malpass-Evans, M. Croad, Y. Rogan, J. C. Jansen, P. Bernardo, F. Bazzarelli and N. B. McKeown, *Science*, 2013, **339**, 303–307.
47 X. Zhu, C. L. Do-Thanh, C. R. Murdock, K. M. Nelson, C. Tian, S. Brown, S. M. Mahurin, D. M. Jenkins, J. Hu, B. Zhao, H. Liu and S. Dai, *ACS Macro Lett.*, 2013, **2**, 660–663.
48 H. A. Patel, S. H. Je, J. Park, Y. Jung, A. Coskun and C. T. Yavuz, *Chem.–Eur. J.*, 2013, **19**, 1–10.
49 X. C. Xu, C. S. Song, B. G. Miller and A. W. Scaroni, *Ind. Eng. Chem. Res.*, 2005, **44**, 8113–8119.
50 B. Chen, N. W. Ockwig, A. R. Millward, D. S. Contreras and O. M. Yaghi, *Angew. Chem., Int. Ed.*, 2005, **44**, 4745–4749.
51 F. Schuth and W. Schmidt, *Adv. Mater.*, 2002, **14**, 629–638.
52 C. A. M. Abella, M. Benassi, L. S. Santos, M. N. Eberlin and F. Coelho, *J. Org. Chem.*, 2007, **72**, 4048–4054.
53 M. G. Rabbani and H. M. El-Kaderi, *Chem. Mater.*, 2012, **24**, 1511–1517.
54 P. Nugent, Y. Belmabkhout, S. D. Burd, A. J. Cairns, R. Luebke, K. Forrest, T. Pham, S. Q. Ma, B. Space, L. Wojtas, M. Eddaoudi and M. J. Zaworotko, *Nature*, 2013, **495**, 80–84.

 